Estimation of electrical conductivity models using multi-coil rigid-boom electromagnetic induction measurements

Carrizo Mascarell, Maria; Werthmüller, Dieter; Slob, Evert

DOI
10.1016/j.cageo.2024.105732

Publication date
2024

Document Version
Final published version

Published in
Computers and Geosciences

Citation (APA)
Carrizo Mascarell, M., Werthmüller, D., & Slob, E. (2024). Estimation of electrical conductivity models using multi-coil rigid-boom electromagnetic induction measurements. *Computers and Geosciences*, *193*, Article 105732. https://doi.org/10.1016/j.cageo.2024.105732

Computers & Geosciences 193 (2024) 105732

Contents lists available at ScienceDirect

Computers and Geosciences

journal homepage: www.elsevier.com/locate/cageo

Research paper

Estimation of electrical conductivity models using multi-coil rigid-boom electromagnetic induction measurements

Maria Carrizo Mascarell *, Dieter Werthmüller, Evert Slob

Faculty of Civil Engineering and Geosciences, Delft University of Technology, Delft, The Netherlands

ARTICLE INFO

Keywords:
Frequency domain electromagnetics
Inversion
Electromagnetic induction

ABSTRACT

Electromagnetic induction measurements from multi-coil configuration instruments are used to obtain information about the electrical conductivity distribution in the subsurface. The resulting inverse problem might not have a unique and stable solution. In that case, a local inversion method can be trapped in a local minimum and lead to an incorrect solution. In this study, we evaluate the well-posedness of the inverse problem for two and three-layered electrical conductivity models. We show that for a two-layered model, uniqueness is ensured only when both in-phase and quadrature data are available from the measurements. Results from a Gauss–Newton inversion and a lookup table demonstrate that the solution space is convex. Furthermore, we demonstrate that for even a simple three-layered model, the data contained in such measurements are insufficient to reach a correct or stable solution. For models with more than 2 layers, independent prior information is necessary to solve the inverse problem. The insights from the numerical examples are applied in a field case.

1. Introduction

Near-surface geophysical technologies are increasingly being used to estimate the electrical conductivity of the subsurface as a way to better understand soil and groundwater properties. A commonly used geophysical technique for this purpose is the electromagnetic induction method (EMI). EMI can be used for a wide range of environmental and hydrogeophysical applications such as soil characterization (Moghadas and Christiansen, 2020), locating contaminants (de Oliveira et al., 2020), evaluation of shallow aquifers (Kiflai and Whitman, 2023), and detection of buried objects (Thiesson et al., 2018).

The non-destructive and cost-effective advantages of EMI instruments make them valuable for characterizing shallow subsurface properties. EMI instruments enable rapid data collection across extensive areas, facilitating quick acquisition of information. Consequently, there is a need to promptly transform this data into a model interpretation of the subsurface. The ability to generate near real-time accurate estimations of subsurface electrical conductivity would turn the collected measurements into an effective decision-making tool.

However, this is not a trivial task. The relationship between the electrical conductivity of the subsurface and the measurements obtained by the EMI instrument is non-linear. For this reason, the inverse problem is usually solved either by making a linear approximation of the solution, which is not feasible for situations with large induction number (Beamish, 2011; Delrue et al., 2020), or iteratively as an optimization problem. Some examples of the optimization approach to obtain layered electrical conductivity models are given by Monteiro Santos et al. (2011), Deleersnyder et al. (2020) and Klose et al. (2022). This inverse scheme requires computing time to perform the forward function iteratively, which might not be practical for near real-time estimation. Moreover, the inverse problem is non-unique, which makes the outcome of the inversion by iterative forward modeling strongly depend on the chosen initial model.

In the following study, we present in Section 2 in detail how we compute the EMI instrument responses using the method described by Ward and Hohmann (1987) for magnetic dipoles over a horizontally, n-layered halfspace. In Section 3 we describe two estimation algorithms: the global search method using a lookup table and the Gauss–Newton inversion. In Section 4 we evaluate both methods using numerical exercises for 2-layered and 3-layered earth models, with different electrical conductivity distributions. We investigate the uniqueness of the solution when in-phase and/or quadrature components of the measurements are available. We also analyze the stability of the solutions for noise presence in the data. From the results of these exercises, we discuss the limitations of the measurements and the methods to obtain a unique solution for 3-layered earth models. Finally, we show the usefulness of the measurements in a field data case assuming a 2-layered earth.

* Corresponding author.
E-mail address: m.e.carrizomascarell@tudelft.nl (M. Carrizo Mascarell).

https://doi.org/10.1016/j.cageo.2024.105732
Received 18 January 2024; Received in revised form 17 September 2024; Accepted 17 September 2024
Available online 23 September 2024

2. Background

The EMI instrument consists of two components: a transmitter coil T_x and a receiver coil R_x. The system uses as a source an alternating current flowing in the transmitter coil to create a primary magnetic field H^{p}, where the magnetic dipole is perpendicular to the transmitter coil plane T_x. This time-varying flux produces an electromotive force inducing eddy currents in the conductive materials of the subsurface, which generate a secondary magnetic field H^{s}. The time-varying fluxes of the magnetic fields H^{p} and H^{s} pass through the receiver coil, inducing a voltage that can be measured by the instrument. Since the primary field H^{p} is known, EMI instruments can provide the mutual impedance ratio between H^{s} and H^{p}, which contains information about the subsurface conductivity.

The solutions of the mutual impedance ratio for diffusive electromagnetic fields for loop-loop configurations over a horizontally layered medium are given by Wait (1982, 104-108) for the horizontal coplanar (H), vertical coplanar (V), and perpendicular (P) coil orientations,

$$Z^{\mathrm{H}} = \frac{H_z^{\mathrm{s}}}{H_z^{\mathrm{p}}} = -s^3 \int_0^\infty R_0 e^{-2\lambda a} \lambda^2 J_0(\lambda s) d\lambda, \tag{1a}$$

$$Z^{\mathrm{V}} = \frac{H_x^{\mathrm{s}}}{H_x^{\mathrm{p}}} = -s^2 \int_0^\infty R_0 e^{-2\lambda a} \lambda J_1(\lambda s) d\lambda, \tag{1b}$$

$$Z^{\mathrm{P}} = \frac{H_x^{\mathrm{s}}}{H_z^{\mathrm{p}}} = s^3 \int_0^\infty R_0 e^{-2\lambda a} \lambda^2 J_1(\lambda s) d\lambda. \tag{1c}$$

Here, a is the height of the instrument above the ground, λ is the radial component of the wavenumber, s is the separation of the coils, R_0 is the earth reflection response, H^{s} and H^{p} represent the primary and secondary magnetic fields, and J_0, J_1 are the Bessel functions of the zeroth and first order, respectively.

Ward and Hohmann (1987, 203–208) proposes that for EMI sensors, where the distance between the transmitter and receiver coils is at least five times larger than the radius of the coils, the coils are considered magnetic dipoles. Moreover, in Equation 4.19 on page 205 of Ward and Hohmann (1987), we find that R_0 can be calculated recursively, beginning with $R_{n+1} = 0$ and

$$R_n = \frac{\frac{\Gamma_n - \Gamma_{n+1}}{\Gamma_n + \Gamma_{n+1}} + R_{n+1} e^{-2\Gamma_{n+1} h_{n+1}}}{1 + \frac{\Gamma_n - \Gamma_{n+1}}{\Gamma_n + \Gamma_{n+1}} R_{n+1} e^{-2\Gamma_{n+1} h_{n+1}}}, \tag{2}$$

where $\Gamma_n = \sqrt{\lambda^2 + \gamma_n^2}$, the vertical wavenumber is defined as $\gamma_n = \sqrt{\omega\mu_0(\mathrm{i}\sigma_n - \omega\epsilon_0)}$, ω is the angular frequency, μ_0 is the magnetic permeability of free space, ϵ_0 is the vacuum permittivity, h is the layer thickness, and σ_n is the electrical conductivity of the nth layer. For a diffusive field approximation $\Gamma_0 = \lambda$. The ground surface is at $z = 0$, and the z-axis points into the ground.

3. Methodology

3.1. Data generation

Considering an earth model with 2 layers, with thickness h_1, we end up with the following equations to solve the reflection coefficient described by Ward and Hohmann (1987):

$$R_2 = 0, \tag{3a}$$

$$R_1 = \frac{\Gamma_1 - \Gamma_2}{\Gamma_1 + \Gamma_2}, \tag{3b}$$

$$R_0 = \frac{\frac{\lambda - \Gamma_1}{\lambda + \Gamma_1} + R_1 e^{-2\Gamma_1 h_1}}{1 + \frac{\lambda - \Gamma_1}{\lambda + \Gamma_1} R_1 e^{-2\Gamma_1 h_1}}. \tag{3c}$$

It is possible to obtain the ratios between primary and secondary magnetic fields for each coil geometry using Eqs. (1a)–(1c) and solving the Hankel transform using a digital filter (Werthmüller et al., 2019).

Table 1
Lookup tables variables.

	Lookup table $D_{2\text{-layers}}$	Lookup table $D_{3\text{-layers}}$
Model parameters $\boldsymbol{m}$	h_1, σ_1, σ_2	h_1, h_2, σ_1, σ_2, σ_3
Number of model parameters M	3	5
Number of layers	2	3
σ range	10–2000 mS/m	10–2000 mS/m
h range	0.1–7 m	0.15–5 m
Number of samples N	121	51
Number of models simulated N^M	1,771,561	345,025,251

This forward operator is fast and easy to compute, generating quickly a large range of possible 1D earth models and storing them in a lookup table.

We assume the model parameters to be $\boldsymbol{m} = [\sigma_1, \sigma_2, h_1]$, where σ_1, σ_2 are the electrical conductivities of the 2 layers, and h_1 is the thickness of the first layer. We use Eqs. (3a)–(3c) to calculate the response R_0 and subsequently compute the ratios $Z^{\mathrm{H}}, Z^{\mathrm{V}}$ and Z^{P} using Eqs. (1a)–(1c) for an EMI system shown in Fig. 1. Each ratio is a complex number where the real part is called in-phase or **IP**, and the imaginary part is called quadrature or **Q**. For each model, we compute the data $\boldsymbol{d} = [\mathbf{Q}^{\mathrm{H}}, \mathbf{IP}^{\mathrm{H}}, \mathbf{Q}^{\mathrm{V}}, \mathbf{IP}^{\mathrm{V}}, \mathbf{Q}^{\mathrm{P}}, \mathbf{IP}^{\mathrm{P}}]$ for the combination of three different offsets, obtaining 18 data values. We then simulate the data measurements for a large range of possible electrical conductivities sampled on a logarithmic scale and possible thicknesses. Finally, the corresponding synthetic data are stored in the lookup table $D_{2\text{-layers}}$ (see Table 1).

We proceed in the same manner, for an earth model with 3 layers, where the model parameters are given by $\boldsymbol{m} = [\sigma_1, \sigma_2, \sigma_3, h_1, h_2]$, with $\sigma_1, \sigma_2, \sigma_3$ being the electrical conductivities of the 3 layers, and h_1, h_2 being the thicknesses of the first layer and second layer (see Table 1, $D_{3-layers}$).

3.2. Global search (GS)

After storing the pre-computed solutions in a lookup table, we perform a global search for the data acquired in each position. This search minimizes the misfit between the acquired data $\boldsymbol{d}_{\mathrm{true}}$ and the data $\boldsymbol{d}_i$ stored in the lookup table $\boldsymbol{D}$. The minimum misfit yields the index of the corresponding best estimate for the electrical conductivity model,

$$\boldsymbol{m}_i = \left\| \boldsymbol{d}_{\mathrm{true}} - \boldsymbol{d}_i \right\|^2 \tag{4}$$

3.3. Gauss–Newton inversion (GN)

The gradient-based optimization scheme uses the Gauss–Newton method to solve non-linear least square problems (Nocedal and Wright, 1999, p. 259–262) to minimize the following objective function:

$$\|\boldsymbol{W}_d(\mathcal{F}(\boldsymbol{m}) - \boldsymbol{d})\|_2^2 + \alpha \|\boldsymbol{W}_m(\boldsymbol{m} - \boldsymbol{m}_0)\|_2^2, \tag{5}$$

where the forward operator $\mathcal{F}(\boldsymbol{m})$ uses Eqs. (1a)–(1c), $\boldsymbol{W}_d$ and $\boldsymbol{W}_m$ are the data weighting and model constraint weighting matrices, $\boldsymbol{m}_0$ is the initial model and α is a regularization term. The Gauss–Newton scheme to minimize this equation updates the model $\Delta\boldsymbol{m}_k$ in the kth iteration using:

$$(\boldsymbol{J}^T \boldsymbol{W}_d^T \boldsymbol{W}_d \boldsymbol{J} + \alpha \boldsymbol{W}_m^T \boldsymbol{W}_m) \Delta\boldsymbol{m}^k = \boldsymbol{J}^T \boldsymbol{W}_d^T \boldsymbol{W}_d (\Delta\boldsymbol{d}^k) - \alpha \boldsymbol{W}_m^T \boldsymbol{W}_m (\boldsymbol{m}^k - \boldsymbol{m}^0), \tag{6}$$

where $\boldsymbol{J} = \frac{\partial \mathcal{F}(\boldsymbol{m})}{\partial \boldsymbol{m}}$, $\Delta\boldsymbol{d}^k = \boldsymbol{d} - \mathcal{F}(\boldsymbol{m}^k)$ and $\Delta\boldsymbol{m}^k = \boldsymbol{m}^k - \boldsymbol{m}^{k-1}$. This is solved using a conjugate-gradient least squares solver (Günther et al., 2006), implemented in the *pyGIMLi* package (Rücker et al., 2017).

To evaluate the prediction accuracy we calculate the normalized root mean squared error (RMSE) between true and estimated 1D models

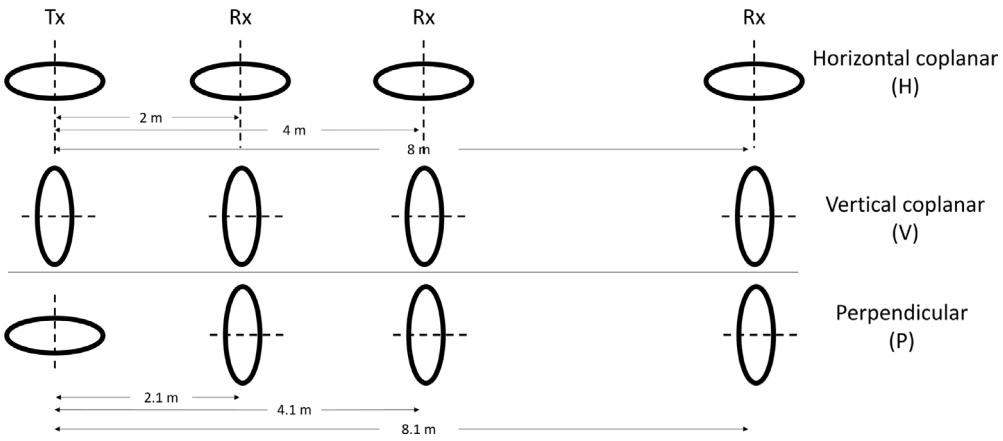

Fig. 1. EMI system.

obtained with the global search method and the optimization approach separately for the σ and h model parameters, as follows:

$$\mathrm{RMSE}(\boldsymbol{m}_{\mathrm{true}}, \boldsymbol{m}_{\mathrm{pred}}) = \sqrt{\frac{\sum_{i=0}^{M-1}(m_{\mathrm{true}} - m_{\mathrm{pred}})^2}{M}}, \tag{7}$$

where $\boldsymbol{m}_{\mathrm{true}}$ is the true model and $\boldsymbol{m}_{\mathrm{pred}}$ is the predicted model.

4. Results and discussion

We start by presenting the estimation of electrical conductivity models on several synthetic datasets of 1D EMI measurements representing a stitched 2D section, using the GS and GN methods. These synthetic datasets were generated using the forward operator discussed in Section 2 (Eqs. (1a)–(1c)). In the following analysis, we investigate for the 2-layered earth whether **IP** and **Q** data are needed to find the correct estimations or if having only **Q** or **IP** data is sufficient. Furthermore, we investigate whether the solution space is convex, containing a unique minimum. We apply this analysis to a 3-layered earth as well.

4.1. 2-layered earth

The estimation methods presented in Section 3 are used for predicting electrical conductivity models in eight numerical cases with different electrical conductivity contrasts (see Table 2). Each case uses twenty 1D synthetic earth models with the same conductivity values for both layers but with increasing thicknesses of the first layer, from 3.25 m to 5.15 m. These are noise-free tests. We present two main cases: (A1) Top resistive layer, (A2) Top conductive layer. It is important to note that while these models fall within the simulated ranges of the lookup table, the exact values are not included in it (See the ranges in Table 1). In the global search (GS) workflow, we found for each 1D model the corresponding model with the best data fit in the lookup table. The obtained models are compared with estimated models using the Gauss–Newton inversion (GN). For the GN method, an initial homogeneous model is set with $\boldsymbol{m}_0 = [3\ \mathrm{m}, 500\ \mathrm{mS/m}, 500\ \mathrm{mS/m}]$, and the regularization parameter is set to $\alpha = 0$.

The results for cases A1-3 and A2-3 are presented in Fig. 2. In each case panel, the true 1D models are in the top row, the GS results are in the left column and the GN results are in the right column. the relative difference of each result is in the third row, and in the fourth- and fifth rows the **Q** and **IP** data fit is shown. The models were estimated using both **IP** and **Q** data values. For all A1 cases, the estimated models using both GS and GN methods show accurate results (see Table 3). The GN produces better results than the GS method because the lookup table was created with discrete steps, in which the true model is not included, giving only the best available model.

Table 2
2-layered earth numerical cases.

Subcase	A1: Top resistive layer		A2: Top conductive layer	
	Top EC [mS/m]	Bottom EC [mS/m]	Top EC [mS/m]	Bottom EC [mS/m]
1	20	200	200	20
2	20	400	400	20
3	20	800	800	20
4	20	1600	1600	20

However, for the A2 cases, both the GS and GN method shows a poor estimation of the bottom resistive layer which worsens with increasing contrast in the electrical conductivity values and with greater thickness of the top conductive layer. Figures of the estimated results for all cases are presented in the Supplementary Material.

In Fig. 3 case A1-3 is estimated using the GS and GN methods described using either the **Q** or **IP** component of the measurements only. The estimated models show good results for both methods. The results of case A1-3 show that when all data is used both GS and GN result in an accurate estimation of the lower conductive layer. Using only **Q** data values produces reasonably good estimates. Interestingly, with **Q**-data both layers are well estimated, whereas with the **IP** data, the conductive layer is better estimated.

On the other hand, in Fig. 4 for case A2-3, both GS and GN methods using **Q** data only produce poorer estimations, especially of the lower resistive layer. The estimation of the electrical conductivity of the resistive layer worsens with increasing contrast (see Table 3). Using **IP** data only also describes better the upper conductive layer.

In both cases, it is clear that the data is more sensitive to the conductive layer than the resistive one. The results shown in this section indicate that **IP** data is sensitive to the conductivity of the model and combined with **Q** measurements produces better estimates in both the GS and GN than using **Q** data alone. It is clear then, that EMI data is sensitive to the conductive layer and that using both **Q** and **IP** increases the chance to better estimate the 2-layered model. These results will be further analyzed in Section 4.1.1.

Apart from the instrument depth sensitivity, a thick conductive first layer attenuates the electromagnetic field more than a resistive first layer, and signal strength is important for deep targets. This can be seen in Fig. 4 from the fact that neither method with **Q** or **IP** data only cannot predict the conductivity of the lower resistive layer

4.1.1. Solution space analysis

To analyze the reasons behind the results in the previous section, we sample the solution space and study different cross-sections for the model in position $x = 10$ m, presented in Figs. 5 and 6. In these figures, it is clear that in case A1-3 the GS and GN methods can find a unique

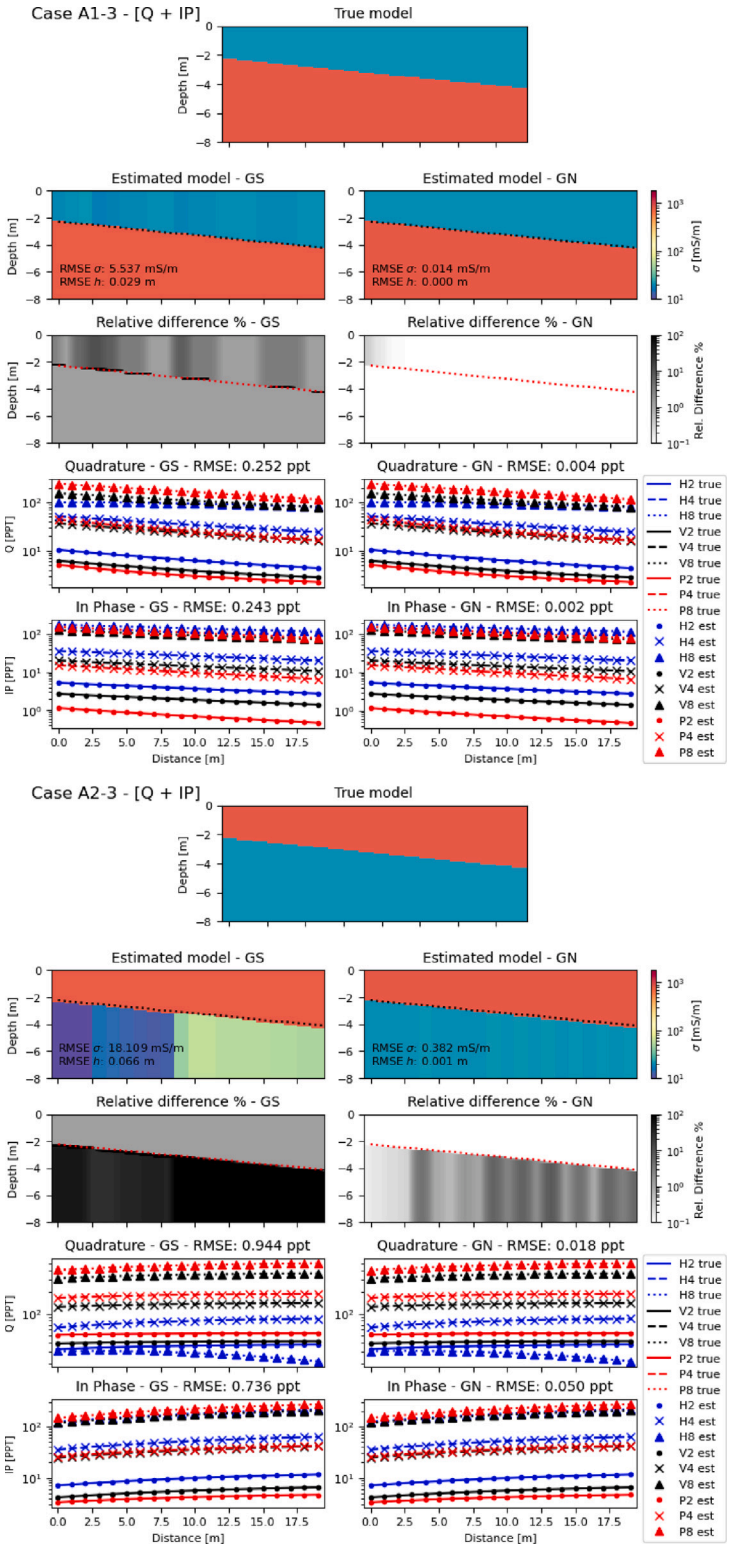

Fig. 2. 2-layered earth: Models estimated using Q and IP data. Top row: true model. Left column: results using GS (Global search). Right column: results using GN (Gauss–Newton inversion) method. Third row: relative difference of the electrical conductivity of the estimated models. Fourth and fifth row: fit between the true and simulated data for the estimated models.

minima. In case A2-3 the GN method is able to find the minima, but there is also a large area of the solution space that has very low NRMSE values which could present a problem when there is noise present in the data. This means that in cases where the subsurface has an upper conductive layer, finding the minima could depend on the data quality.

In A2 cases using **Q** data only for the estimations, we obtained poor results in examples A2-1 and A2-2. In Fig. 6 we observe that the error space using **Q** data only has a saddle shape, which is also the case for cases A2-1 and A2-2 (see Supplementary Material). For this reason, depending on the initial model chosen the estimation might follow a

Table 3
RMSE table: 2-layered models.

Method	Case	Data: Q +IP				Data: Q			Data: IP		
		RMSE σ [mS/m]	RMSE h [m]	RMSE Q [ppt]	RMSE IP [ppt]	RMSE σ [mS/m]	RMSE h [m]	RMSE Q [ppt]	RMSE σ [mS/m]	RMSE h [m]	RMSE IP [ppt]
Global search (GS)	A1-1	0.725	0.34	0.112	0.038	6.087	0.133	0.093	2.534	0.11	0.01
	A1-2	4.213	0.061	0.246	0.161	12.102	0.102	0.094	9.333	0.164	0.022
	A1-3	5.537	0.029	0.252	0.243	12.198	0.027	0.19	7.993	0.054	0.026
	A1-4	0.75	0.017	0.251	0.333	0.646	0.017	0.271	4.039	0.018	0.025
	A2-1	1.27	0.064	0.108	0.028	3.073	0.121	0.084	1.294	0.066	0.027
	A2-2	9.325	0.213	0.539	0.113	40.252	0.353	0.432	10.191	0.236	0.114
	A2-3	18.019	0.066	0.944	0.736	43.39	0.216	0.903	8.511	0.115	0.307
	A2-4	5.174	0.018	0.121	0.145	4.174	0.018	0.106	5.619	0.018	0.125
Gauss-Newton (GN)	A1-2	0.035	0	0.013	0.003	0.172	0.003	0.004	2.359	0.076	0.005
	A1-2	0.016	0	0.005	0.002	0.009	0	0.003	8.781	0.165	0.009
	A1-3	0.014	0	0.004	0.002	0.037	0	0.003	16.612	0.125	0.024
	A1-4	0.027	0	0.007	0.003	0.022	0	0.006	88.015	0.257	0.14
	A2-1	0.003	0	0.001	0	965.09	3.788	5.582	0.042	0.001	0.004
	A2-2	0.181	0	0.022	0.03	657.04	3.603	9.151	1.353	0.032	0.023
	A2-3	0.382	0.001	0.018	0.05	51.979	0.264	0.8	1.942	0.019	0.031
	A2-4	1.012	0	0.045	0.102	5.301	0.019	0.105	3.648	0.01	0.088

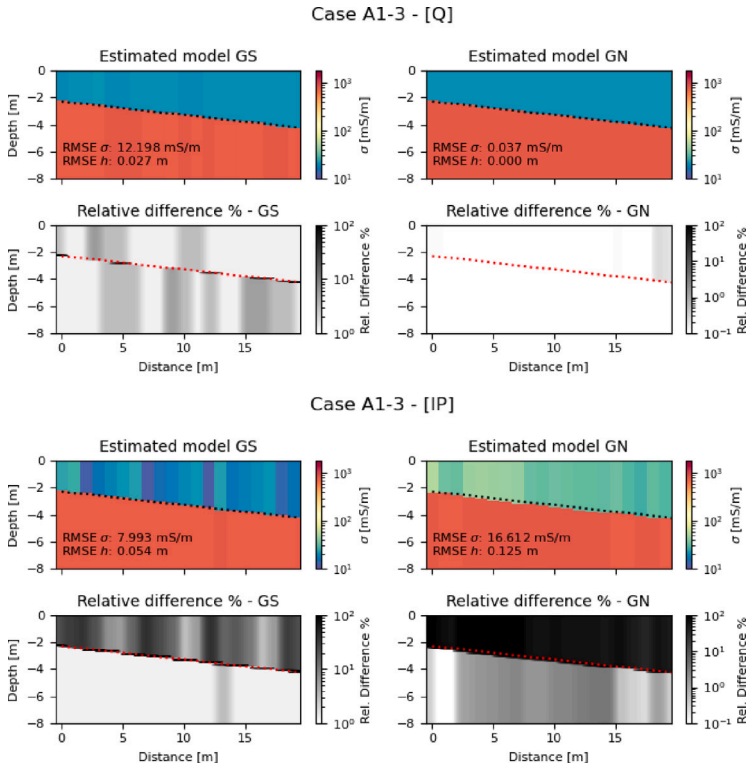

Fig. 3. 2-layered models A1-3 estimated using **Q** component (top row) or **IP** component only (bottom row).

path with a direction to a local minima instead of the true minima. This explains the inaccurate results seen in Fig. 4.

In Fig. 6 the solution space cross-sections for case A2-3 using **IP** data only for the estimations. The cross-sections show the solution space has a valley shape that allows the GN method to find the convex area where the true minima can be found. For this reason, we can obtain better estimations of an upper conductive 2-layered earth model using **IP** data only. This suggests that the **IP** data is relevant and should be included in EMI estimations. The **Q** + **IP** cross-sections represent the combination of the overlapping of the **Q** and **IP** cross-sections

4.1.2. Noise analysis

EMI measurements can be affected due to a low signal-to-noise ratio (Delefortrie et al., 2014). Therefore, we evaluate the performance of the methods against random noise. The random noise is created as in the following equation:

$$\tilde{\boldsymbol{d}} = \boldsymbol{d}(\boldsymbol{I} + \boldsymbol{R}\epsilon) \tag{8}$$

where the data $\tilde{\boldsymbol{d}}$ is the noisy data, $\boldsymbol{I}$ is the identity matrix, $\boldsymbol{R}$ is a diagonal matrix of random values with a standard normal distribution of zero mean and unit standard deviation $\boldsymbol{R} = \text{diag}(\mathcal{N}(0,1))$, and ϵ is the error fraction.

In Fig. 7 we observe the estimation with GS and GN methods of a 1D model using data with 10% random noise in 100 instances. For A1 cases the estimation results show a good estimation of the lower conductive layer and a larger variance in the conductivity and thickness of the upper resistive layer. The variance of the thickness decreases for higher contrast in the electrical conductivity. For A2 cases the estimations cannot accurately describe the lower resistive layer using either the

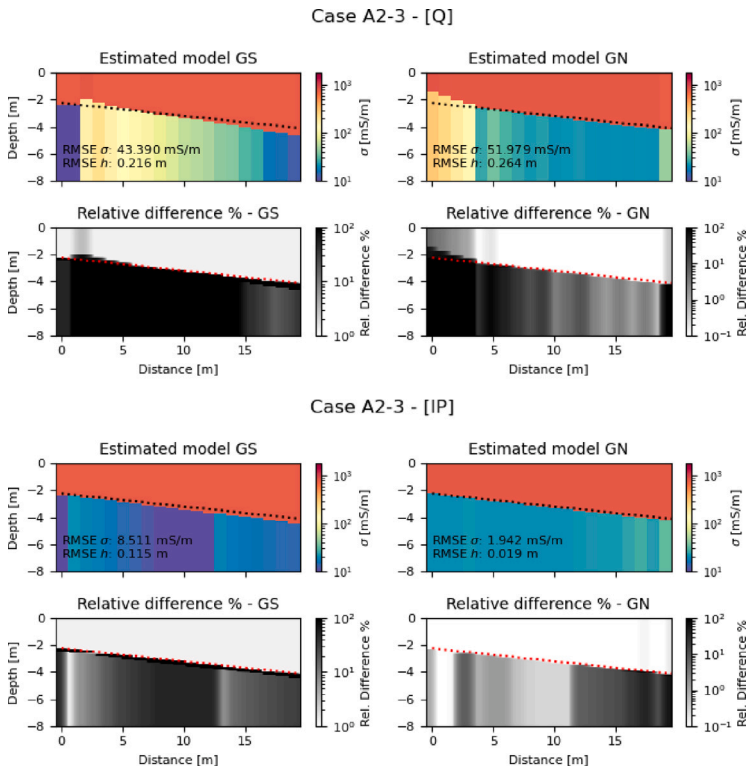

Fig. 4. 2-layered models A2-3 estimated using **Q** component (top row) or **IP** component only (bottom row).

GS or GN method. The results worsen with increasing contrast in EC between the upper and lower layers. The variance of the conductivity values for the resistive layer ranges several orders of magnitude in the worst case (A2-4). This can be explained by looking at Fig. 6 where a no-noise case can find the true minima using the GN method, but the solution space shows a wide low misfit valley where by adding only 10% of noise to the measurements the method finds very different models that can explain the data within the noise range. This means, that for an upper-conductive 2-layered earth model even when using both **Q** and **IP** measurements, the model estimations might not be accurate depending on the noise levels.

A1 and A2 cases estimated with noisy data are shown in the Supplementary Material. The RMSE increases for both estimation approaches for increasingly noisy data. The resulting 1D model estimations are worse for the case of the upper conductive layer (A2). The GS and the GN approach focus on solving the conductive part of the models.

4.2. 3-layered earth

We analyze a more complex inverse problem by increasing the number of model parameters to a 3-layered model and studying whether the inversion methods can reach a unique solution. We show the results of the estimations for the GS and GN methods using twenty 3-layered 1D earth models in a stitched 2D section. The estimations were carried out using both **Q** and **IP** components in the measurements. We present eight cases: (B1) Four conductive middle layer cases in a resistive background. (B2) Four resistive middle layer cases in a conductive background. For all examples, the middle layer thickness increases from 1.5 m to 3.5 m (see Table 4). As in the previous case, while these models fall within the simulated ranges of the lookup table, the exact values are not included in it. For the Gauss–Newton inversion, an initial homogeneous model is set with $\boldsymbol{m}_0 = [3\text{ m}, 3\text{ m}, 100\text{ mS/m}, 100\text{ mS/m}, 100\text{ mS/m}]$, and the regularization parameter $\alpha = 0$.

The results for the conductive middle layer case B1-3 and the resistive middle layer case B2-3 are presented in Fig. 8. The RMSE values for all the cases are indicated in Table 5. All estimated models are shown in the Supplementary Material. The GS and GN methods' performance differs in B1-3 and B2-3 cases. In case B1-3, the GS method can properly estimate the thickness and conductivity of the first and second layers. The estimation of the third layer, however, is the least accurate. On the other hand, GN the model predictions are quite poor.

For the B2-3 case, neither the GS nor the GN could predict the true models with sufficient accuracy. Both the GS and GN could predict the conductivity of the first layer, and the thickness of the first layer for some positions. However, the resistive body is not well determined in conductivity or thickness. These results will be better explained in the following sections.

4.2.1. Initial model m_0

Using the GN estimation method we must choose an initial model m_0 to initialize the minimization of Eq. (5). Depending on the shape of the error space, the choice of m_0 might affect the resulting estimation, as was shown in Fig. 6 for the A2 case using **Q** data only. In Fig. 9 we show the estimated models for the position $x = 10$ m in case B1-3 using different initial models m_0. From these results, it is clear that the estimated models differ greatly depending on the initial model. This indicates that estimating a 1D 3-layered model using **Q** and **IP** measurements might not be feasible.

4.2.2. Error space analysis

When increasing the number of layers from 2 to 3 we find that both the GS and GN schemes have trouble estimating the 1D models. To explain this better, let us focus on Fig. 10 where we study the 1D model in position $x = 10$ m of the 3-layered case B1-3. In the figure, the left panel contains the true and estimated 1D model, and the right panel shows a 3D cloud of points of the solution space (corresponding to the solutions computed in the lookup table). In the solution space cloud, the low **NRMSE** values correspond to a large volume, with models from wide ranges of different thicknesses and electrical conductivities. The path taken by the GN method shows that the minimization is trapped in a local minima far from the true solution. From this analysis above,

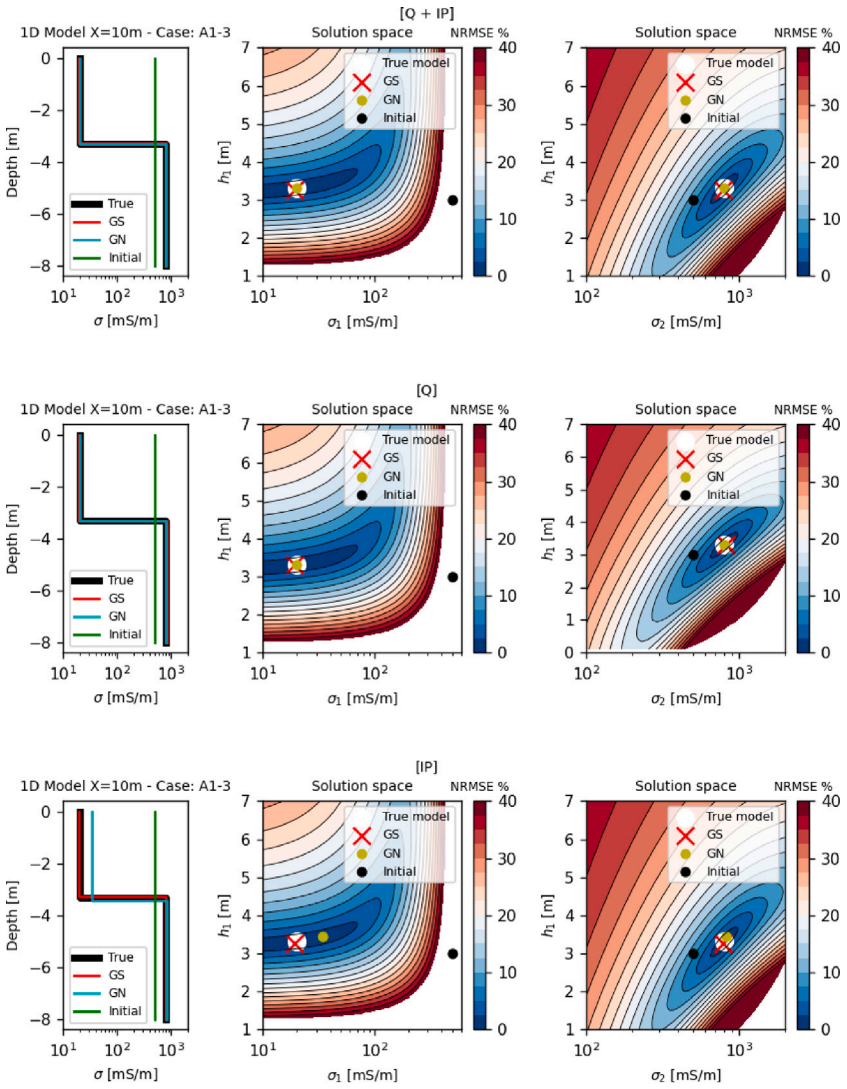

Fig. 5. Cross-sections of the solution space for case A1-3. Top panel: using **Q** + **IP** data. Middle panel: **Q** data. Lower panel: **IP** data. In each panel the estimated model is shown in the left column, the cross-section for fixed σ_2 to the estimated value in the middle column, and in the rightmost column the cross-section for a fixed σ_1 equal to the estimated value. In the cross-sections, the true model is indicated with a white dot which corresponds to the only minima present. The GS and GN methods can find the minima.

Table 4
3-layered earth cases.

Subcase	B1: Conductive middle layer		B2: Resistive middle layer	
	Background EC [mS/m]	Middle layer EC [mS/m]	Background EC [mS/m]	Middle layer EC [mS/m]
1	20	200	200	20
2	20	400	400	20
3	20	800	800	20
4	20	1600	1600	20

there are two main insights: First, different 3-layered earth models can explain the measurements within a small error range, translating into an unstable solution. Second, depending on the initial model the path taken by the GN method might differ and thus, result in very different estimations of the earth models.

4.3. Limitations of the methods

The GN method is usually applied to estimate earth models with this type of electromagnetic measurement. However, as we have seen in the previous results, in a 2-layered earth for the configuration of the instrument described, it is necessary to use both **Q** and **IP** measurements, which are not available in some instruments already existent in the industry. Additionally, for a 3-layered case, even with **Q** and **IP** components available, the success while using this method depends highly on the initial model chosen. Moreover, many possible models that differ greatly from each other explain the data within a 5% **NRMSE** of the measurements, which makes the solution to this inversion problem quite unstable.

On the other side, the GS method for a 2-layered earth can determine an acceptable estimate, depending on how many models are pre-computed and whether the ranges of the variables contain the true earth model. However, for a 3-layered earth, the GS is only moderately successful for a middle conductive layered earth. Due to memory limitations (see Table 6), the variable sampling ranges of the pre-computed models are coarser for a 3-layered case, which translates

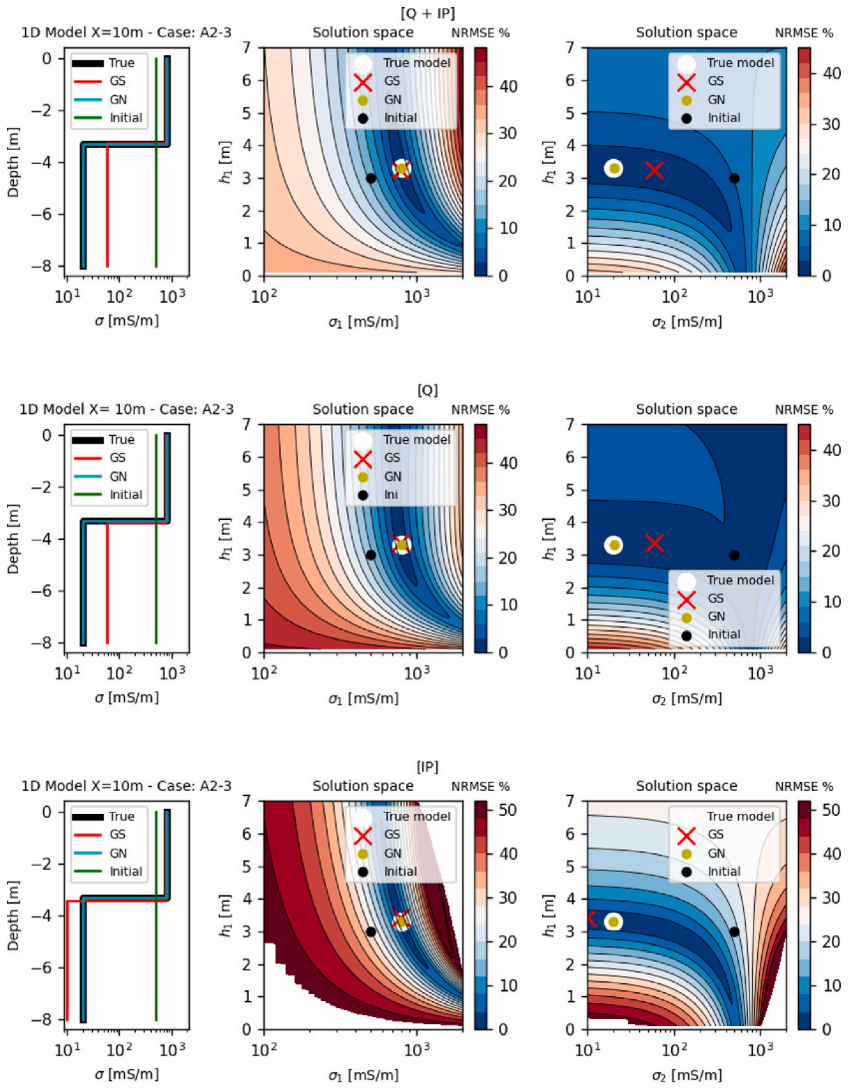

Fig. 6. Cross-sections of the solution space for case A2-3. In the cross-sections, the true model is indicated with a white dot which corresponds to the minima in a wide area of small NRMSE. The GS estimated model falls close due to sampling, estimating slightly different models to the true model.

Table 5
RMSE table: 3-layered models.

Method	Case	Data: Q +IP			
		RMSE σ [mS/m]	RMSE h [m]	RMSE Q [ppt]	RMSE IP [ppt]
Global search (GS)	B1-1	7.839	0.203	2.364	0.927
	B1-2	11.933	0.130	4.108	2.608
	B1-3	11.696	0.059	5.617	6.277
	B1-4	29.378	0.048	5.273	11.540
	B2-1	8.705	0.668	0.287	0.041
	B2-2	62.567	0.846	0.239	0.068
	B2-3	187.354	0.805	1.207	0.652
	B2-4	243.118	0.509	0.510	0.284
Gauss-Newton (GN)	B1-1	0.838	0.011	2.361	0.929
	B1-2	11.732	0.065	4.084	2.548
	B1-3	119.373	1.163	24.458	10.798
	B1-4	493.350	0.925	22.945	13.675
	B2-1	15.888	0.251	2.314	4.306
	B2-2	7.423	0.049	0.112	0.052
	B2-3	253.467	1.188	1.176	2.327
	B2-4	846.107	3.928	12.368	11.324

to less accurate estimations. In the middle resistive case, the estimations worsen, due to the low sensitivity of the instrument to resistive bodies under a conductive layer. We used 48 cores of an AMD Rome 7742 CPU and 45 GB of RAM memory.

In the following section, we analyze the benefit of using the GS method as a previous step of the GN method to increase the chance of success in estimating 3-layered earth models.

4.4. Global search + Gauss–Newton

The previous results showed that for a 3-layered earth, the GN method is limited by the initial model. If there is no previous knowledge of the subsurface, the GN method estimation could be very far from the true subsurface. We study if for such a case using the GS method to obtain an initial estimate could be beneficial. The method begins by doing a global search in the pre-computed solutions present in the lookup table obtaining a 1D estimated model. Afterward, this estimated model can be used as the initial model $\mathbf{m}_0$ in the Gauss–Newton inversion, providing a better opportunity for the minimization to reach the appropriate minima in the error space. In Fig. 11 the results of the two previous estimation methodologies and the new combination of GS and GN for the 3-layered earth numerical examples are shown.

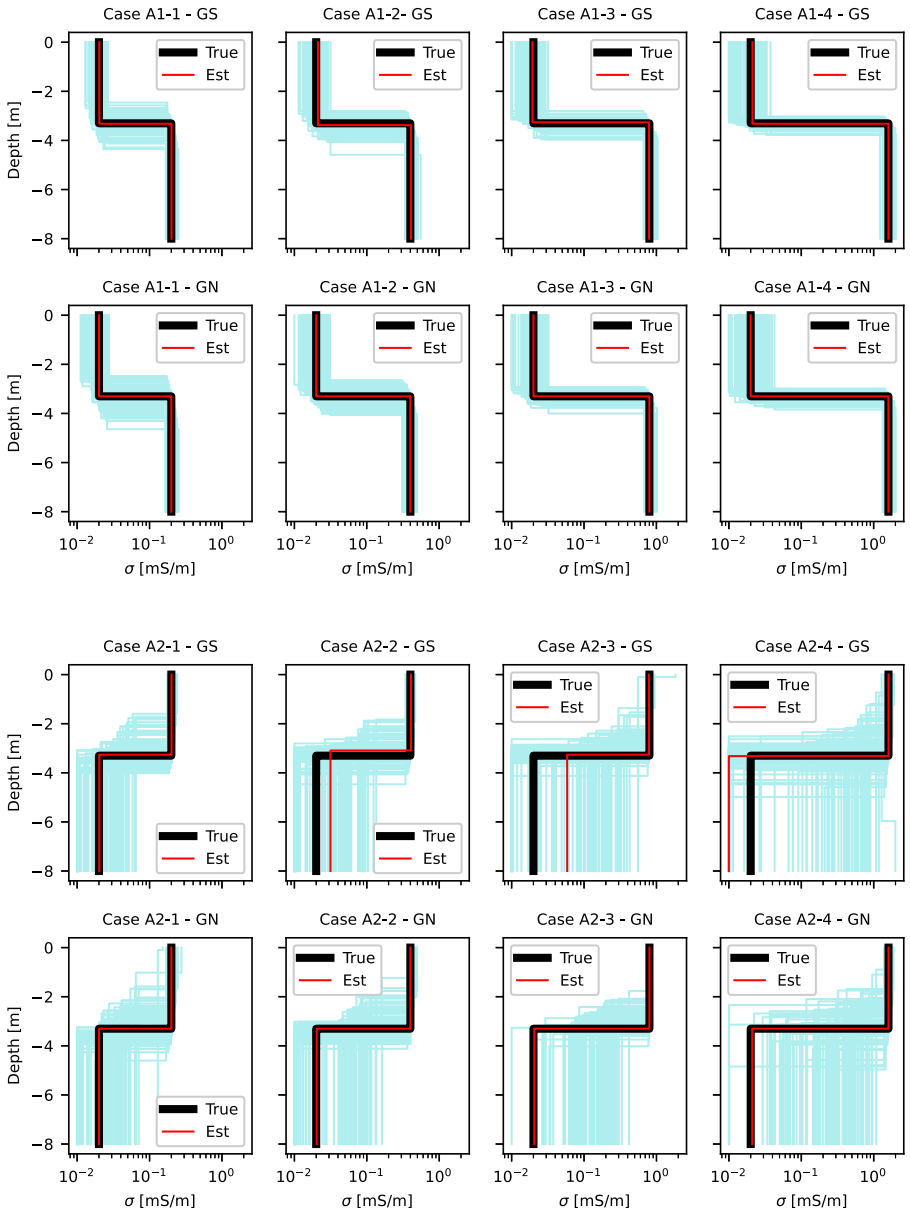

Fig. 7. Results for the GS and GN method results using the data measurements for a 1D model with added 10% random noise in 100 instances. The estimated models are presented in pale turquoise lines. The true and no-noise estimated models are presented in black and red lines, respectively. In A1 cases the results show a wider variance in the estimation of the top resistive layer. For A2 cases (top conductive) the results show that the bottom resistive layer varies widely. This suggests that the estimation problem in these cases is quite unstable due to noise presence in the data.

Table 6
Computing parameters of the GS method for increasing n number of layers.

n number of layers	Parameters	Samples per parameter	Number of pre-computed measurements	Computing time for all measurement	Memory resources	Time to estimate 1 model
2	3	121	1,771,561	57 s using 8 cores	230 Megabytes	0.24 s
3	5	51	345,025,251	3.08 h using 48 cores	45 Gigabytes	48 s

In both cases B1-3 and B2-3, we can see that for some 1D models, there is a slight improvement in the detection of the middle layer and the **RMSE** decreases. For the resistive middle layer cases (B2-3), there is an improvement, however, the estimates still differ from the true

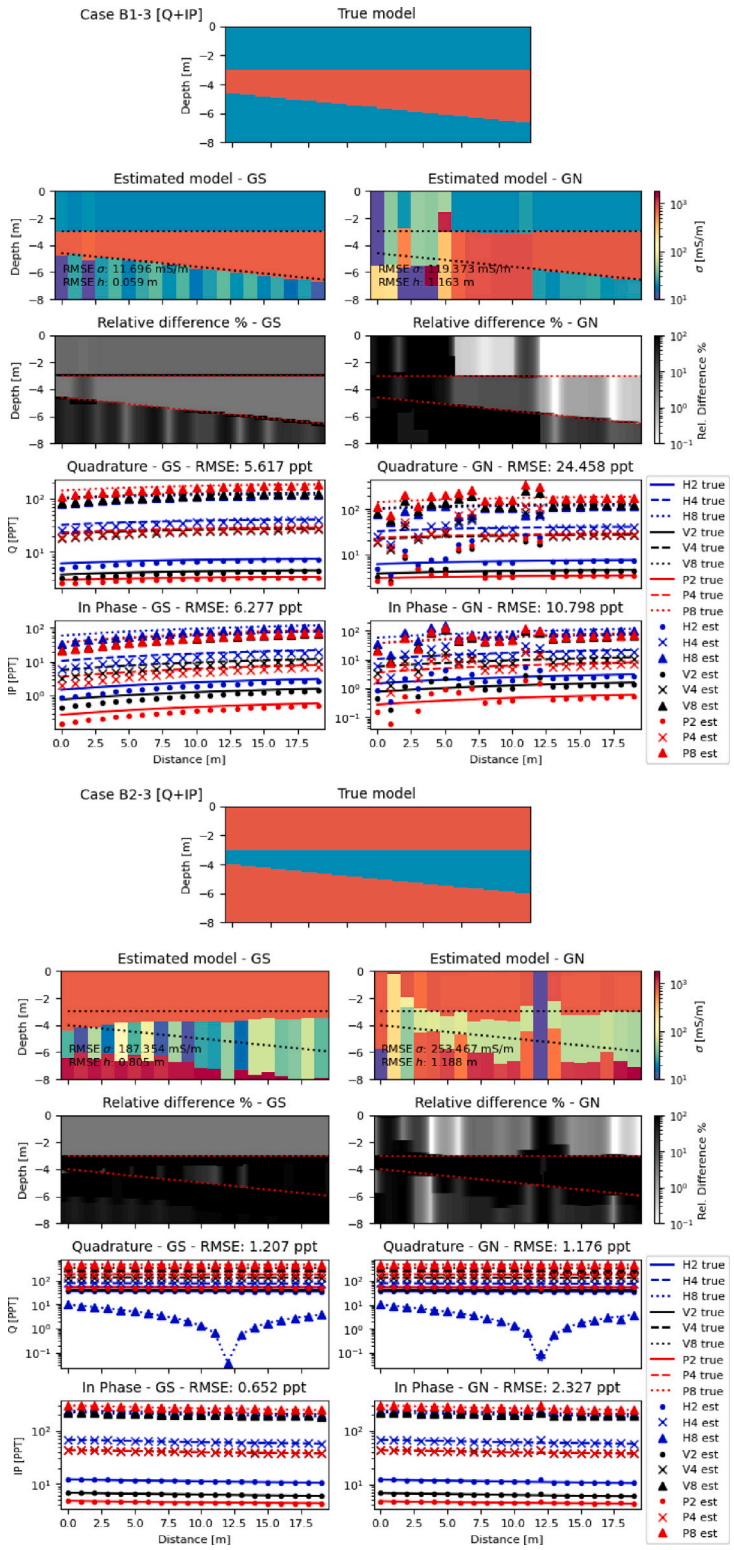

Fig. 8. 3-layered earth: Models estimated using Q and IP data. Top row: true model. Left column: results using GS. Right column: results using GN. Third row: relative difference of the estimated models. Fourth and fifth row: fit between the true and simulated data.

models. This brings out the point that the GN method is still in some cases unable to find the true solution for 3-layered cases. Moreover, the GS method also cannot always find the proper solution due to several models satisfying a certain data misfit criterion, then the GN method cannot be expected to improve the estimation further. This further suggests that such data cannot be used for 3-layered model estimation without prior information.

4.5. Field data case

We use an electromagnetic induction dataset acquired in Ackerdijkse Plassen, The Netherlands (see Fig. 12) containing 1850 measurements. The data is pre-processed removing noisy spikes. Following the instrument developer's recommendations, we do not use the **IP** measurements for offsets under 4 m in the estimations (Taylor, 2023).

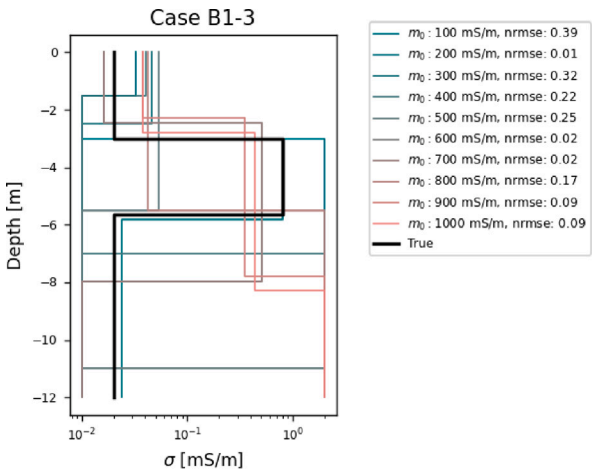

Fig. 9. Estimation of a 1D 3-layered earth models in case B1-3 using GN method with different m_0.

We use only the H and V loop-loop configurations. We assume the area to have a 2-layered shallow subsurface (up to 10 m depth) based on lithology samples taken from nearby boreholes.

We carry out 2-layered 1D model estimations from the field measurements using the two approaches: global search (GS) and Gauss–Newton (GN) inversion. In Fig. 13 three cross-sections from each estimation methodology are shown. In the first column are the results from the GS method, and in the second column are the results from the GN approach. These cross-sections show that the area holds a top resistive layer with values around 60 mS/m, with a maximum thickness of 6 m, and a bottom conductive layer with values around 120 mS/m. Both methods show similar results. There are differences in the thickness of the first layer in a topographic low where a water stream is present in the field. This is better observed in the maps in Fig. 14 where the estimated model parameters are shown in the area.

From Fig. 14 we can see that the distribution of the electrical conductivity and thicknesses generally does not show great changes in the different methods. The top layer resistivity shows higher conductivity values above the stream feature. The thickness maps show a thickness increase above the stream feature. The misfit **RMSE** between true and simulated data for all measurements acquired is 2.29 ppt and 1.79 for the GS and GN methods, respectively. We can see a slight improvement using the Gauss–Newton inversion methodology. However, the difference is marginal. Therefore, we can deduce that for this 2-layered field case, either method can be used and will reach a satisfactory outcome.

5. Conclusions

In this study, we evaluate the well-posedness of the inverse problem in estimating two-layered and three-layered 1D earth models using multi-coil single-frequency rigid-boom electromagnetic induction measurements. This analysis is carried out using a global search through lookup tables and a Gauss–Newton inversion scheme.

We showed that for a two-layered model, a Gauss–Newton approach is sufficient to find the minimum misfit and estimate the model only when using both quadrature and in-phase data components. Adding the in-phase part to the quadrature part of the measurements increases the amount of information about the subsurface and produces a convex solution space for two-layered earth models. Hence, the inverse problem is well-posed in this case. Moreover, we show the solution is quite stable under the influence of noise, except when the upper layer is more conductive than the lower halfspace.

On the other hand, already for a three-layered noise-free numerical model, the Gauss–Newton method is not able to find the correct model, except when the initial estimate is close to the correct model. This is due to the shape of the solution space, which is rather flat close to the true minimum, and it has multiple local minima where the optimization might get trapped. This suggests that the problem is ill-posed for a three-layered earth due to the solution's non-uniqueness. The global search method might provide better estimations given a sufficient sampling of the pre-computed models in the middle conductive layered earth. Nonetheless, neither method can describe the subsurface precisely for a middle resistive layered earth.

Additionally, we tested an alternative inversion scheme that combines a global search to get an initial estimate before the Gauss–Newton inversion to improve the model estimate through a local search. The scheme was applied to synthetic cases, where the middle resistive layered cases showed little improvement. For finite precision data, the global search cannot improve in reaching the true model because a local minimum can have the same or smaller misfit value than the true solution. This emphasizes the point that the data available for the instrument configuration used in this study are insufficient to determine uniquely and precisely a three-layered 1D earth model without prior knowledge of the subsurface.

CRediT authorship contribution statement

Maria Carrizo Mascarell: Writing – original draft, Visualization, Software, Investigation, Formal analysis, Data curation. **Dieter Werthmüller:** Writing – review & editing, Supervision, Software. **Evert Slob:** Writing – review & editing, Supervision, Methodology, Funding acquisition.

Declaration of competing interest

The authors declare the following financial interests/personal relationships which may be considered as potential competing interests: Evert Slob reports financial support was provided by Rijksdienst voor Ondernemend Nederland (RVO). If there are other authors, they declare that they have no known competing financial interests or personal relationships that could have appeared to influence the work reported in this paper.

Data availability

I have provided data and source codes in the attached file.

Acknowledgments

This project was carried out as part of the WarmingUP Innovation Plan, made possible partially by a subsidy from the Rijksdienst voor Ondernemend Nederland (RVO), The Netherlands in the context of the Meerjarige Missiegedreven Innovatie Programma's (MMIP) subsidy scheme (RVO project number TEUE819001).

Code availability section

Name of the code/library: MC_RB_EM_1D
Contact: m.e.carrizomascarell@tudelft.nl
Hardware: The computations of the 3-layered Lookup table and Global search were performed on the Geoscience and Engineering server at Delft University of Technology. We used 48 cores of an AMD Rome 7742 CPU and 46 GB of memory. All the other computations were performed on an Intel(R) Core(TM) i7-8665U CPU with 8 GB of RAM memory.
Program language: Python
Software required: Python 3
Repository size: 77 MB
Access to data and source codes are available for download at the link: https://github.com/mariacarrizo/MC_RB_EM_1D

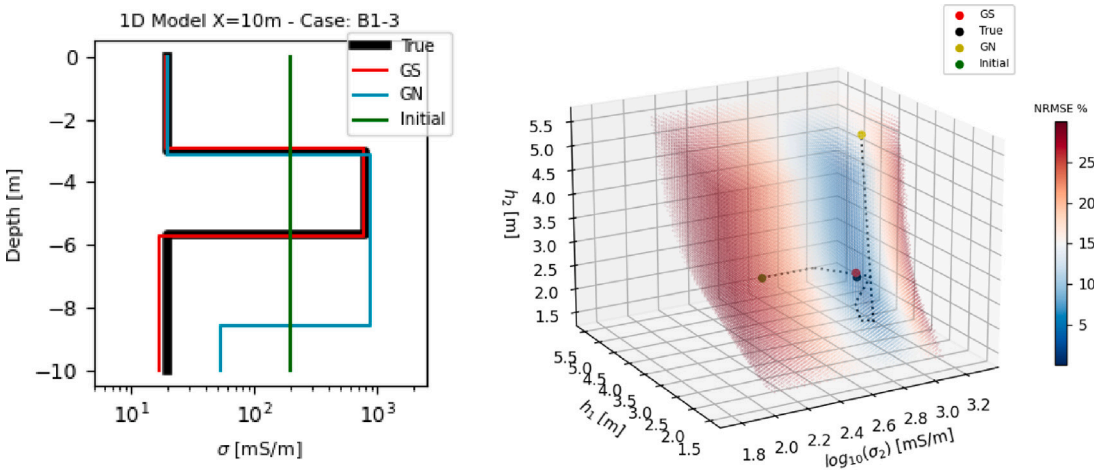

Fig. 10. In the left panel, the true and estimated 3-layered 1D models for cases B1-3 are shown. In the right panel, the solution space cloud points corresponding to the position $x = 10$ m in case B1-3 is shown. The true model in the 3D plot is a black dot, and the GS estimated model is a red dot. The initial model for GN is a green dot, the path of the model updates is a dotted black line, and the final GN estimated model is a yellow dot.

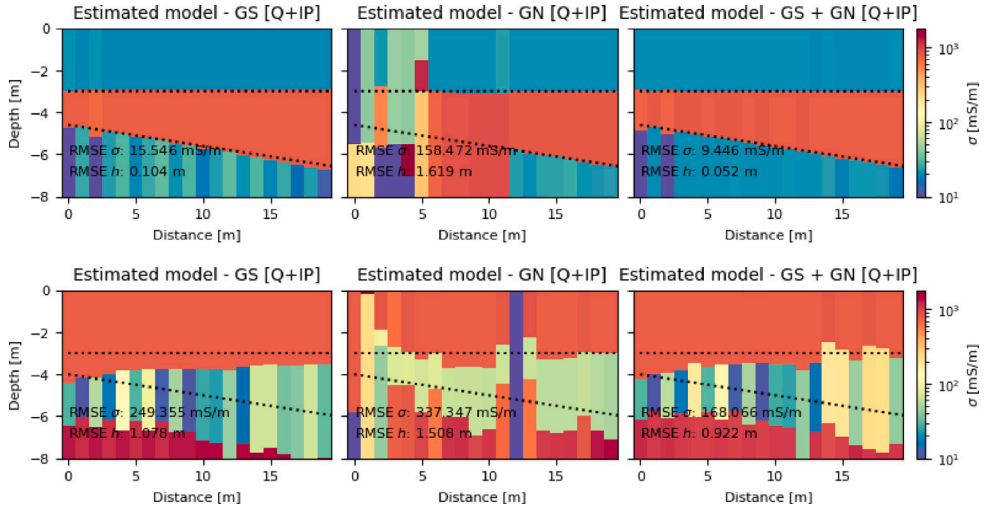

Fig. 11. Global search + Gauss Newton results. Top row: B1-3 case (middle conductive layer). Bottom row: B2-3 case (middle resitive layer). The GS method estimates are in the left column, the GN estimates in the middle column and the combined algorithm results in the right column.

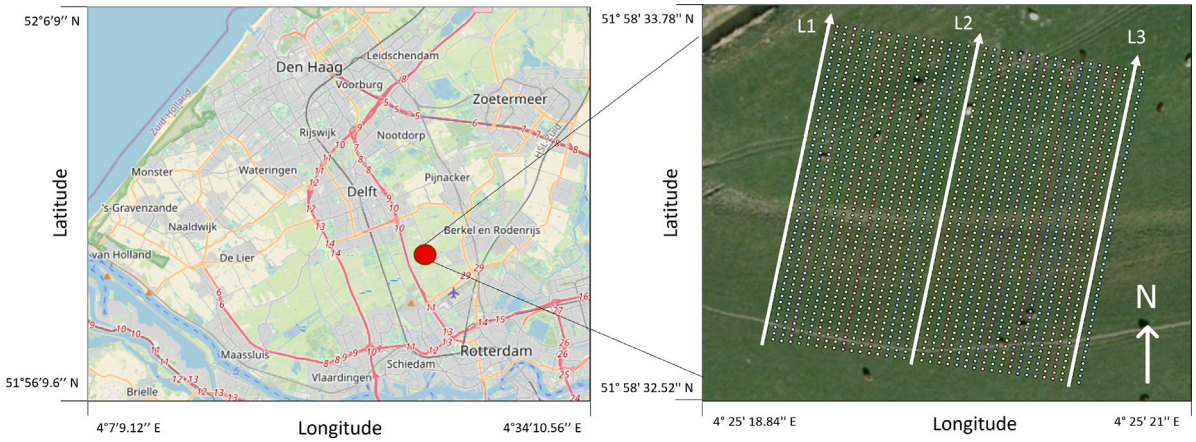

Fig. 12. Study Area: Ackerdijse Plassen, The Netherlands. The cross-sections L1, L2 and L3 are highlighted.

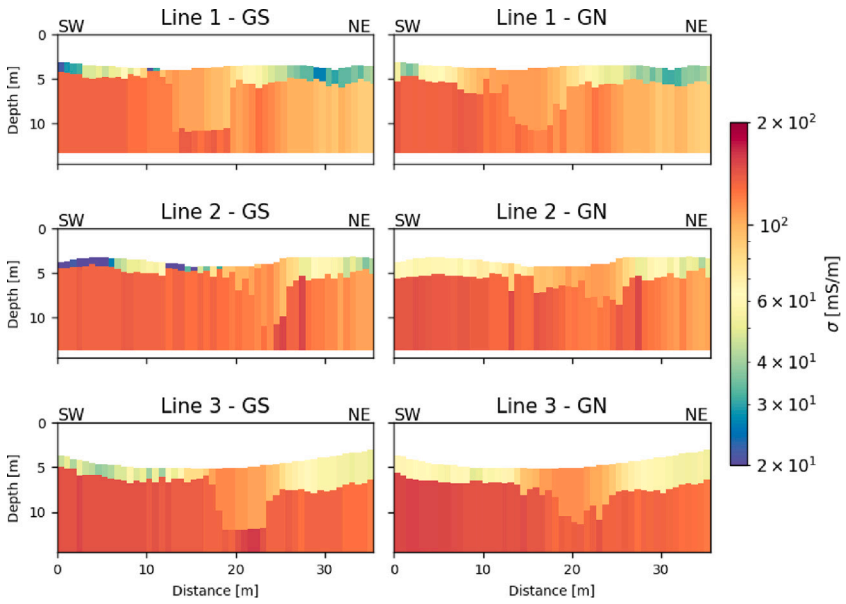

Fig. 13. Cross-sections of estimated models. The estimations show a top resistive layer above a conductive layer. The top layer increases in conductivity around the stream feature present in the satellite image.

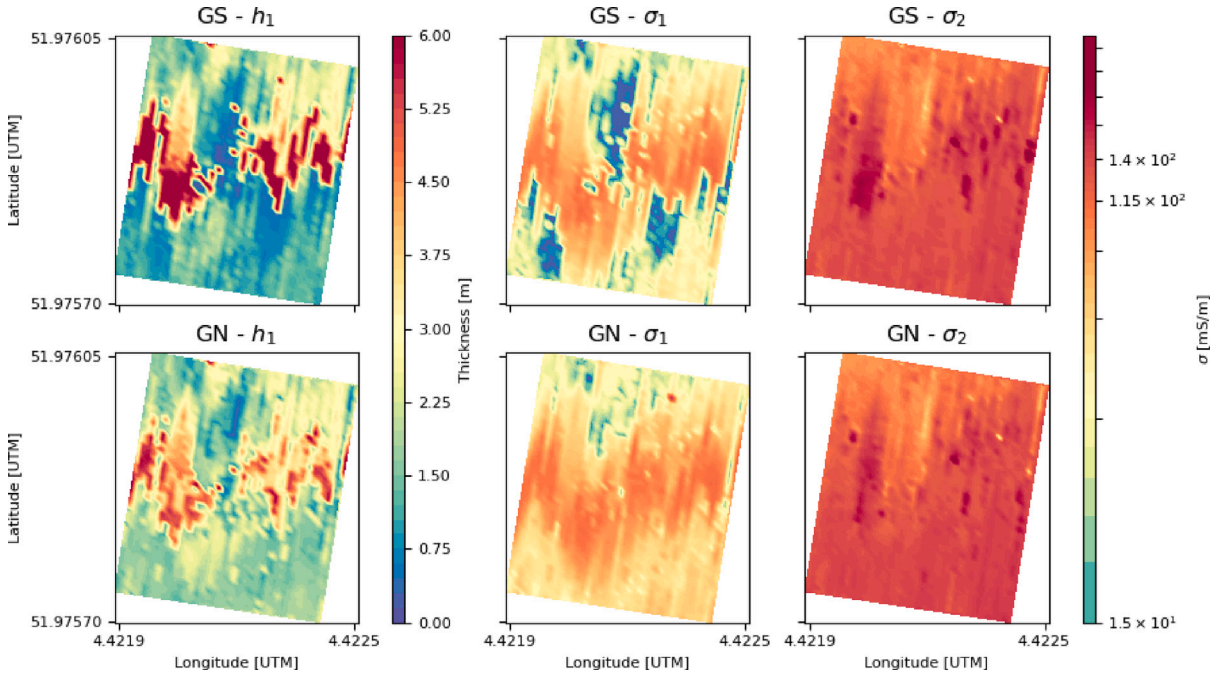

Fig. 14. Maps of estimated models. Top row: Thickness of first layer (h_1). Second row: electrical conductivity of first layer (σ_1). Bottom row: Electrical conductivity of the second layer (σ_2).

Appendix A. Supplementary data

Supplementary material related to this article can be found online at https://doi.org/10.1016/j.cageo.2024.105732.

References

Beamish, D., 2011. Low induction number, ground conductivity meters: A correction procedure in the absence of magnetic effects. J. Appl. Geophys. 75 (2), 244–253. http://dx.doi.org/10.1016/j.jappgeo.2011.07.005.

de Oliveira, L.A., Woodbury, B.L., de Miranda, J.H., Stromer, B.S., 2020. Using electromagnetic induction technology to identify atrazine leaching potential at field scale. Geoderma 375, http://dx.doi.org/10.1016/j.geoderma.2020.114525.

Deleersnyder, W., Maveau, B., Hermans, T., Dudal, D., 2020. Inversion of electromagnetic induction data using a novel wavelet-based and scale-dependent regularization term. Geophys. J. Int. 226 (3), 1715–1729. http://dx.doi.org/10.1093/gji/ggab182.

Delefortrie, S., Saey, T., Van De Vijver, E., De Smedt, P., Missiaen, T., Demerre, I., Van Meirvenne, M., 2014. Frequency domain electromagnetic induction survey in the intertidal zone: Limitations of low-induction-number and depth of exploration. J. Appl. Geophys. 100, 14–22. http://dx.doi.org/10.1016/j.jappgeo.2013.10.005.

Delrue, S., Maveau, B., Dudal, D., 2020. A damped forward EMI model for a horizontally stratified earth. Explor. Geophys. 51 (4), 422–433. http://dx.doi.org/10.1080/08123985.2019.1708717.

Günther, T., Rücker, C., Spitzer, K., 2006. Three-dimensional modelling and inversion of dc resistivity data incorporating topography — II. Inversion. Geophys. J. Int. 166 (2), 506–517. http://dx.doi.org/10.1111/j.1365-246X.2006.03011.x.

Kiflai, M.E., Whitman, D., 2023. Geophysical mapping of freshwater lens in Big Pine Key, Florida: Electromagnetic induction calibration and application. Near Surf. Geophys. 21 (2), 152–167. http://dx.doi.org/10.1002/nsg.12244.

Klose, T., Guillemoteau, J., Vignoli, G., Tronicke, J., 2022. Laterally constrained inversion (LCI) of multi-configuration EMI data with tunable sharpness. J. Appl. Geophys. 196, 104519. http://dx.doi.org/10.1016/j.jappgeo.2021.104519.

Moghadas, D., Christiansen, A.V., 2020. Soil electrical conductivity imaging using a neural network-based forward solver: Applied to large-scale Bayesian electromagnetic inversion. J. Appl. Geophys. 176, 104012. http://dx.doi.org/10.1016/j.jappgeo.2020.104012.

Monteiro Santos, F.A., Triantafilis, J., Bruzgulis, K., 2011. A spatially constrained 1D inversion algorithm for quasi-3D conductivity imaging: Application to DUALEM-421 data collected in a riverine plain. Geophysics 76 (2), B43–B53. http://dx.doi.org/10.1190/1.3537834.

Nocedal, J., Wright, S.J., 1999. Nonlinear least-squares problems. In: Numerical Optimization. Springer New York, New York, NY, pp. 250–275. http://dx.doi.org/10.1007/0-387-22742-3_10.

Rücker, C., Günther, T., Wagner, F.M., 2017. pyGIMLi: An open-source library for modelling and inversion in geophysics. Comput. Geosci. 109, 106–123. http://dx.doi.org/10.1016/j.cageo.2017.07.011.

Taylor, R., 2023. Website of DualEM manufacturer: EM induction. EM Induction https://dualem.com/documents/em-induction/. (Accessed on 21 April 2023).

Thiesson, J., Tabbagh, A., Dabas, M., Chevalier, A., 2018. Characterization of buried cables and pipes using electromagnetic induction loop-loop frequency-domain devices. Geophysics 83 (1), E1–E10. http://dx.doi.org/10.1190/geo2016-0476.1.

Wait, J.R., 1982. Chapter III - Electromagnetic induction and loop–loop coupling. In: Wait, J.R. (Ed.), Geo-Electromagnetism. Academic Press, pp. 101–139. http://dx.doi.org/10.1016/B978-0-12-730880-7.50007-7.

Ward, S.H., Hohmann, G.W., 1987. Electromagnetic theory for geophysical applications. In: Electromagnetic Methods in Applied Geophysics: Volume 1, Theory. Society of Exploration Geophysicists, pp. 131–311. http://dx.doi.org/10.1190/1.9781560802631.ch4.

Werthmüller, D., Key, K., Slob, E., 2019. A tool for designing digital filters for the Hankel and Fourier transforms in potential, diffusive, and wavefield modeling. Geophysics 84 (2), F47 – F56. http://dx.doi.org/10.1190/geo2018-0069.1.